Supplementary Figure S1. Methods of CTC analysis and CTC-associated KM plots

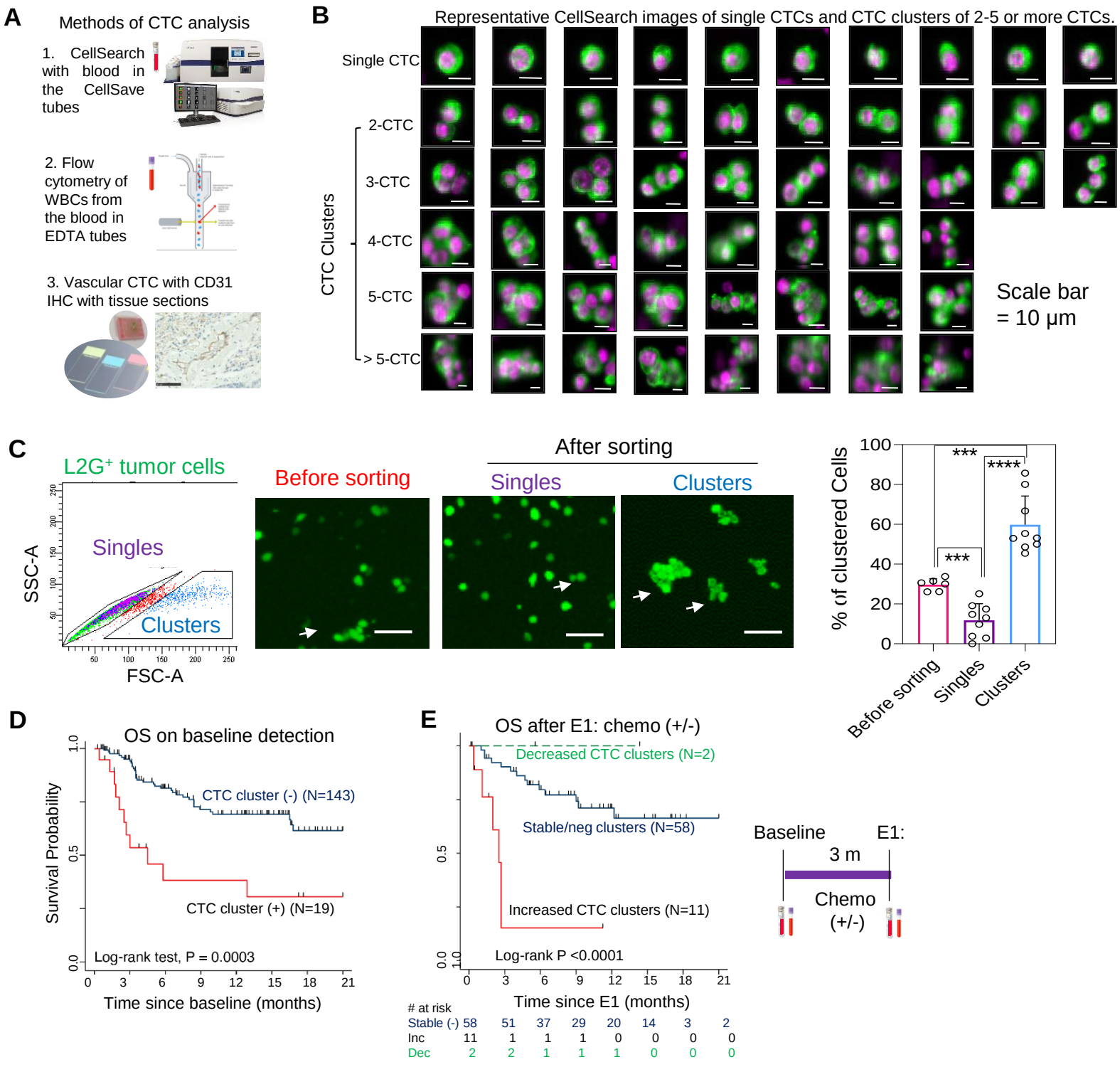

Supplementary Fig. S1. Methods of CTC analysis (CellSearch and flow cytometry) and overall survival of breast cancer patients based on CTCs at the baseline and E1 after treatment.

A. Schematic illustration of three methods for CTC analysis, including CellSearch, flow cytometry, and IHC.

B. Representative CellSearch images of single CTCs and CTC clusters of 2-5 or more CTCs per cluster, detected from the blood of the patients with stage III-IV breast cancer.

C. Flow profile (left panel) with gated singles and clusters, fluorescent images before and after sorting of MDA-MB-231 cells (L2G-labeled) based on SSA and FSC-A channels (middle panels) (scale bar=50 µm), and quantification **(**%) of multi-cellular clusters (two or more cells) within unsorted, sorted singles, and sorted clusters (right panel). Student's *t*-test ***p<0.001, ****p<0.0001.

D-E. The probability of overall survival (OS) by Kaplan-Meier estimates in advanced-stage breast cancer patients with and without detection of CTC clusters by CellSearch analysis at the baseline prior to new treatment (N=162) (D) and at E1 after treatment for combined groups of chemotherapy (+/-) (N=71) (E).

Supplementary Figure S2. Glycosylation profiles of CTCs.

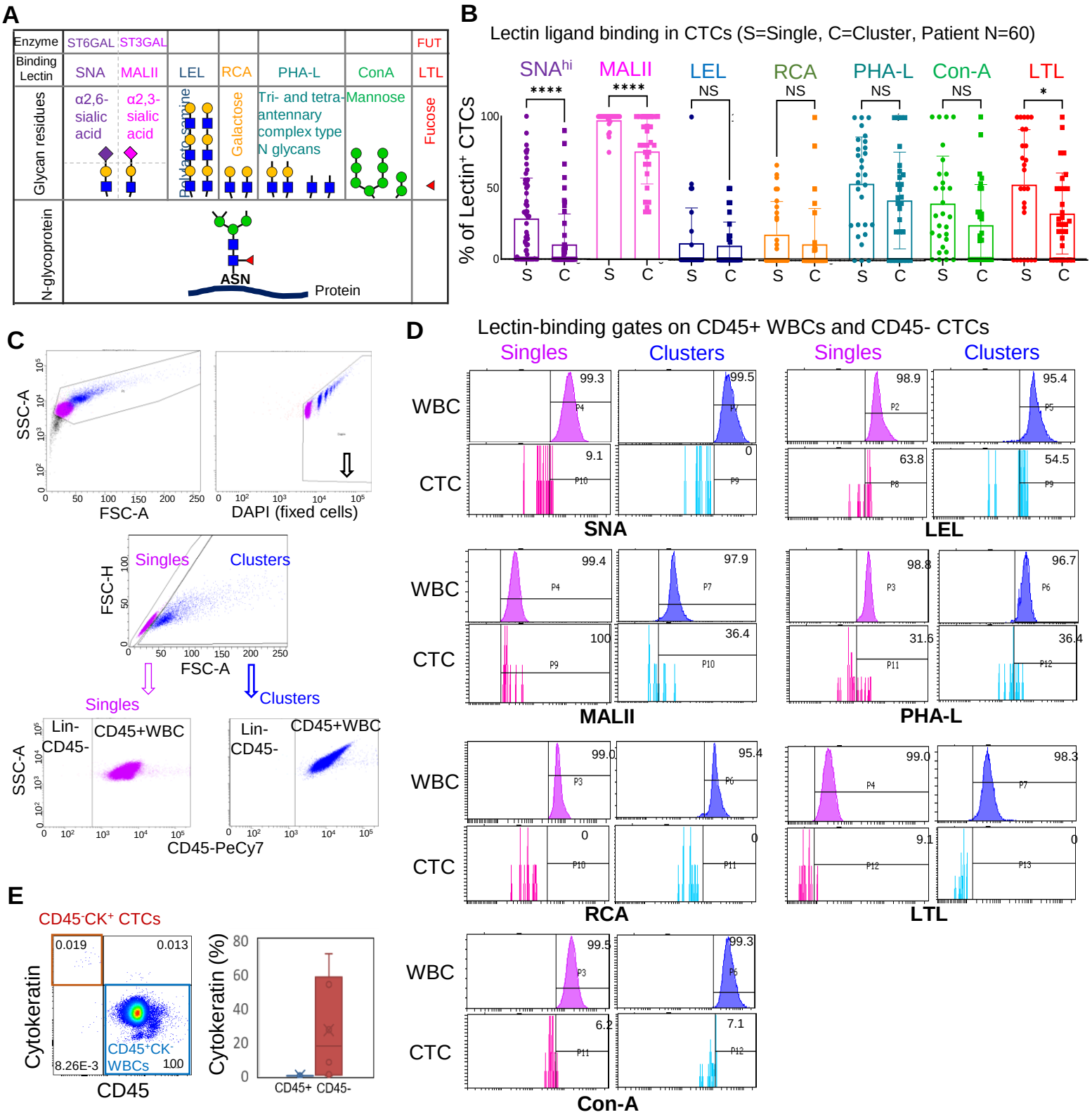

Supplementary Fig. S2. Glycosylation profiles of CTCs in the patient blood (singles and clusters).

A. Diagram of lectin binding carbohydrate structures and respective catalytic enzyme for transfer of N-glycans.

B. Percentage (%) of indicated lectin binding (+ or high) CTCs in the singles (S) versus the clusters (C), as flow detected in the blood of patients with advanced stage III-IV breast cancer. N=60 patients for SNA and N=30 patients for MALII, LEL, RCA, PHA-L, ConA, and LTL. Student's *t*-test via Graphpad ****p ≤ 0.0001, *p ≤ 0.05, and NS=not significant. Data are represented as mean values +/- SD.

C-D. The gating strategies in flow cytometry analyses to isolate single and clustered CTCs (C) and indicated lectin^{high} cells (D) in patient blood samples. Fixed cells were first gated with the size channels SSC-A and FSC-A, then gated for DAPI$^+$ cells with DNA, subsequently divided into singles and clusters by FSC-H and FSC-A, both of which were further gated by CD45. CD45$^+$ WBCs were used for the positive control of indicated lectin-high cells (D). Single cells are shown in pink color and clusters were presented in blue color (WBCs in darker colors and CTCs in lighter colors).

E. The flow profile and cytokeratin (%) in CD45$^+$WBCs and CD45-CK$^+$ CTCs in the blood of a breast cancer patient.

Supplementary Figure S3. Neuraminidase treatment and CD44 on clustering and sialyation

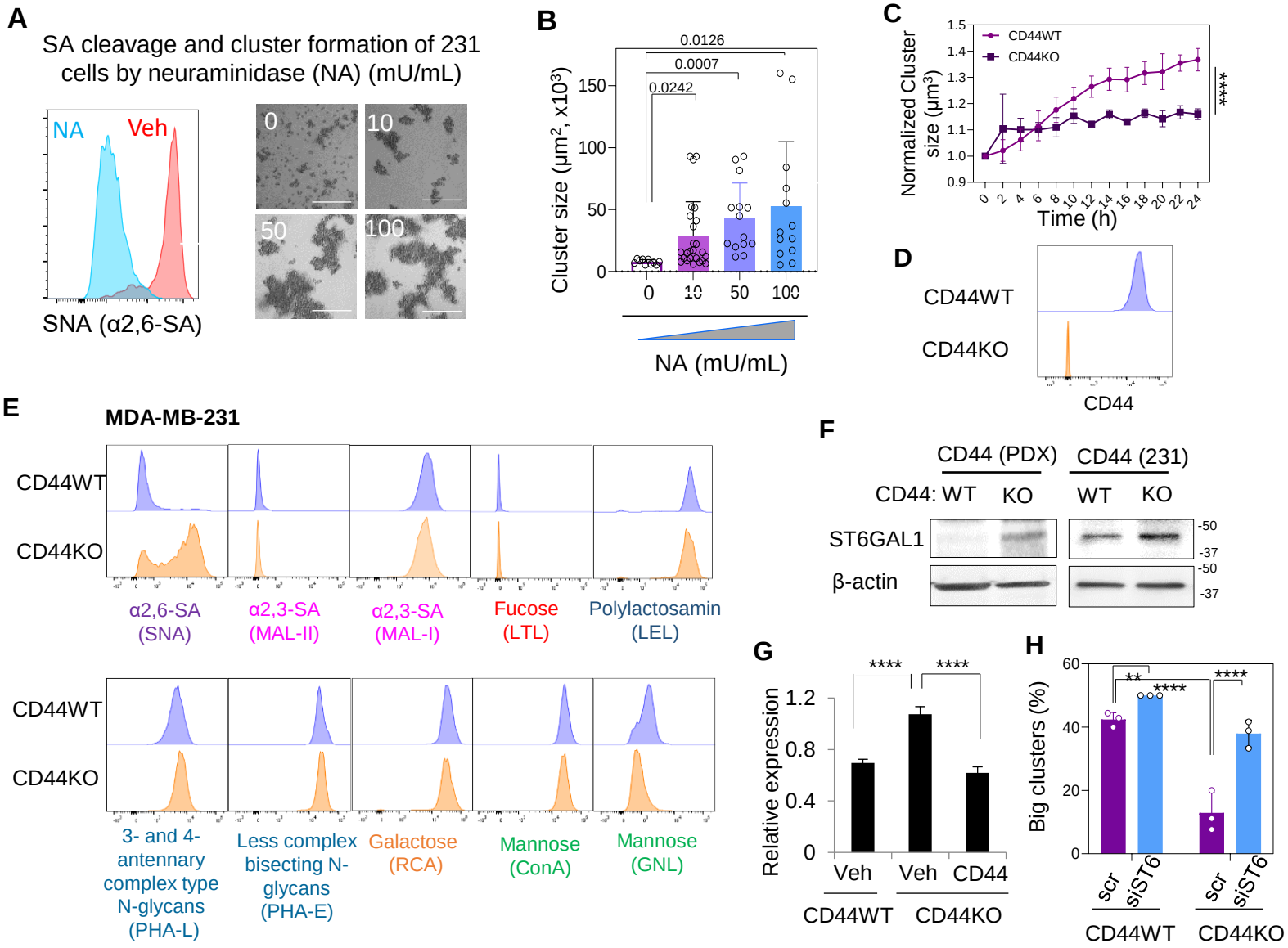

Supplementary Fig. S3. Phenotypic effects of neuraminidase treatment and CD44 depletion on tumor clustering and sialylation.

A. Representative flow histogram of α2,6-SA levels (SNA-binding signals) in the tumor cells treated with vehicle control (Veh) and neuramidinase (NA, 50 mU/mL) (left panel) and representative images of aggregated MDA-MB-231 tumor cell clusters after NA treatment at 0-100 mU/mL for 24 h (scale bars = 500 μm) (right panels).

B. Bar graph of improved tumor cell cluster formation (cluster size) after NA-mediated removal of SA in a dose-dependent manner (0-100 mU/mL). The size of the clusters are measured by ImageJ. Student's *t*-test P values are calculated using GraphPad and 14 experimental replicates with +/- SD are shown.

C. Cluster formation of CD44 -wild type (CD44WT) vs -knockout (CD44KO) cells. Cluster formation was measured by incucyte at indicated time points. ****p>0.0001.

D. The validation of CD44 expression in CD44WT and CD44KO cells by flow cytometry analysis.

E. Flow cytometry profiles of the glycan detected by indicated lectin bindings in CD44WT (cluster forming) and CD44KO (non-cluster forming) cells. The diagram of binding of lectins to carbohydrates is shown in parenthesis which is also shown in ExtendedFig.2A.

F. Western blotting with indicated antibody blotting in CD44WT (WT) and CD44KO (KO) cells.

G. mRNA expression level of ST6GAL1 in CD44WT after vehicle (veh) transfection and in CD44KO cells after veh and standard form CD44 (CD44s) transfection. ****p>0.0001

H. Cluster formation of CD44WT and CD44KO cells after transfection of scramble siRNA (scr) and siST6GAL1. **p>0.01, ****p>0.0001.

Supplementary Figure S4. N-glycomic analysis of α2,6-SA peaks in WT and ST6KO cells

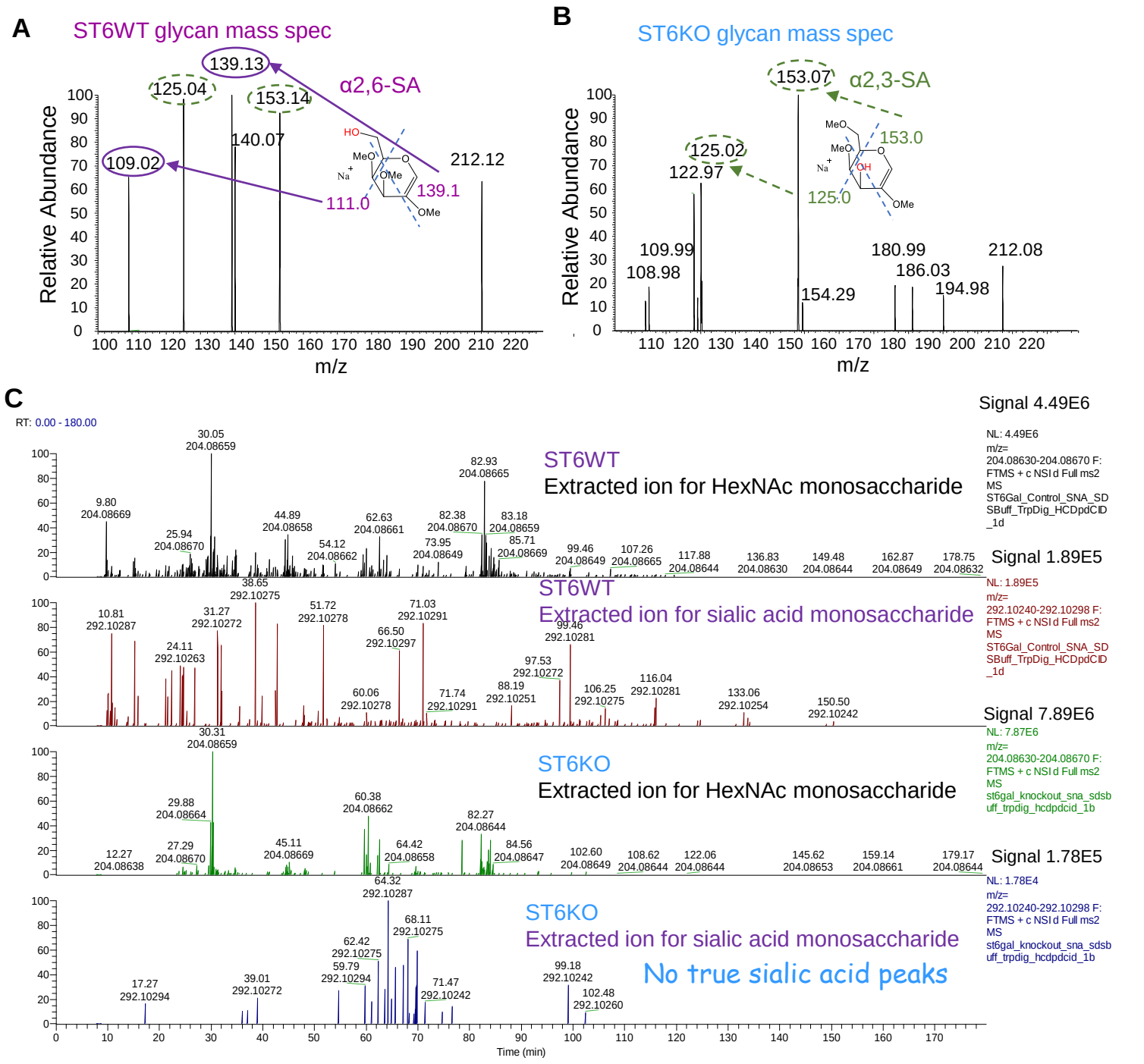

Supplementary Fig. S4. N-glycomic analysis of α2,6-SA peaks in WT and ST6KO MDA-MB-231 cells by LC-MS/MS.

A-B. N-glycomic analysis of ST6GAL1 wild-type (ST6WT) and knockout (ST6KO) cells. Purple circles highlight α-2,6-sialic acid (α2,6-SA) peaks exclusively in WT cells whereas orange circles of α-2,3-sialic acid (α2,3-SA) peaks present in both WT and KO cells. The blue dash lines are depicting the cross-ring fragmentations of monosaccharide (galactose attached to sialic acid) which are leading to signature fragments indicating the linkage of sialic acids.

C. Extracted ion chromatogram from LC-MS/MS spectra of tryptic digest of SDS buffer of eluted glycoproteins from ST6WT and ST6KO cells.

Supplementary Figure S5. Depletion of ST6GAL1 or ST3GAL1 promotes clustering and chemo-evasion

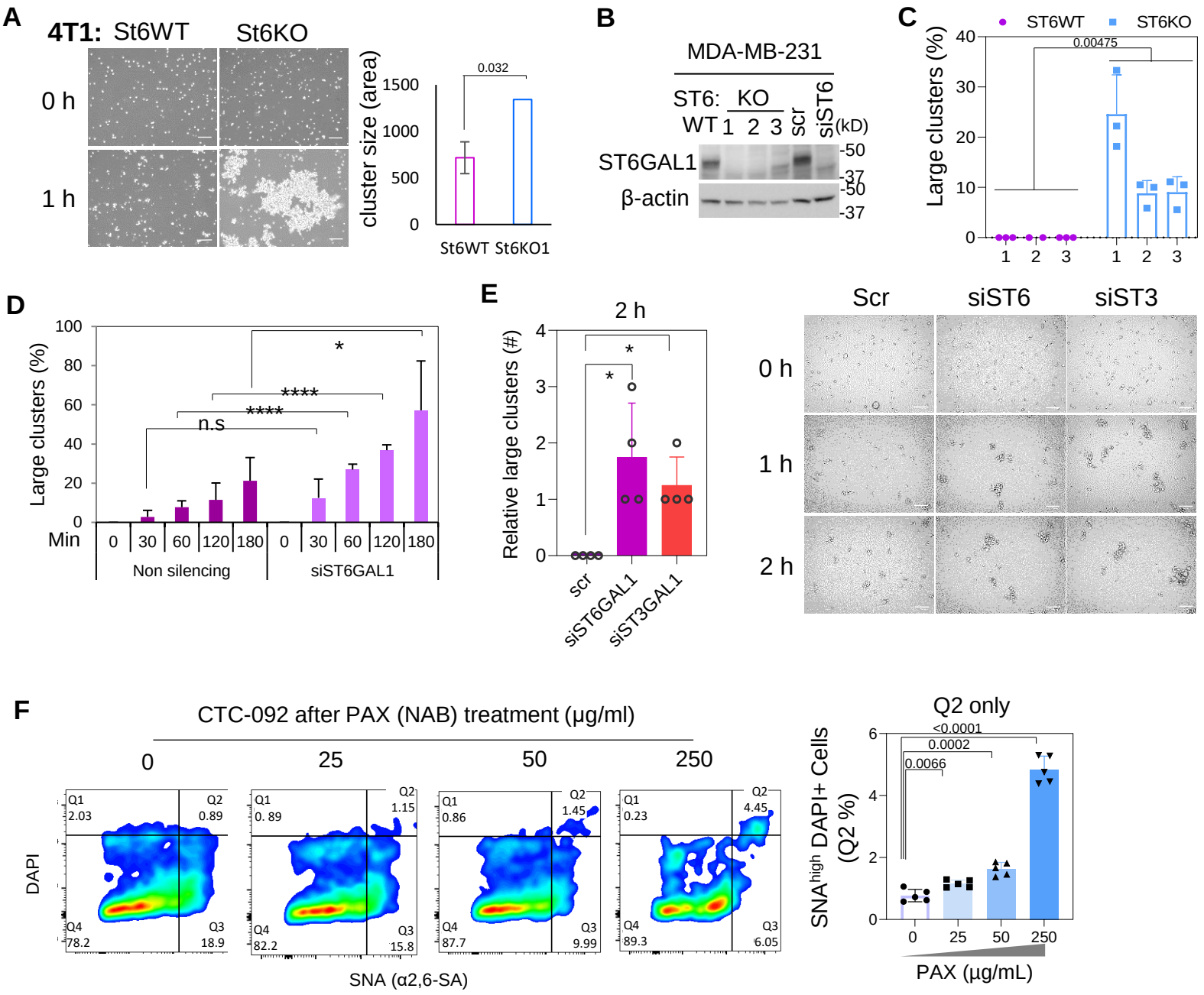

Supplementary Fig. S5. Depletion of ST6GAL1 or ST3GAL1 promotes cluster formation and the viability of CTC092 cells after PAX treatment.

A. Representative images (left panels) and the size of tumor cluster area of mouse tumor 4T1 cells (St6gal1 WT and KO) after 1 hour aggregation. Scale bar = 150 μm, and Student's *t*-test ***p ≤ 0.001

B. Western blotting of ST6Gal1 expression in ST6WT, 3 clones of ST6KO (1, 2, and 3) cells, and the MDA-MB-231 cells transfected with the scrambled siRNAs control (scr) and siST6GAl1 (siST6).

C-D. Proportion (%) of large clusters (>11 or 30 cells) formed by ST6 WT/KO cells (C) and the cells with ST6 knockdown by siRNAs (D). Student's *t*-test *p<0.05 and **** p<0.0001

E. Left panel: large cluster counts within 2 hours (h) of MDA-MB-231 cells transduced with scramble RNA (scr), siRNA of ST6GAL1 (siST6GAL1, siST6), and siRNA of ST3GAL1 (siST3GAL1, siST3). Student's *t*-test *p<0.05. Right panels display representative images of cell clusters at 0, 1, and 2 h. Scale bar=100μm.

F. Flow profiles (left panels) and quantification (right) of SNA-high DAPI^{+} cell death (Q2 subset) of CTC-PDX-092 cells after treatment of nano-albumin bound paclitaxel, PAX-Nab) at different concentrations (0-250 μg/mL). The graph shows the quantification of chemo-induced death, SNA+DAPI+ cells (right panel). Student's *t*-test p values = 0.0066, 0.0002, and <0.0001 as indicated.

Supplementary Figure S6. ST6GAL1 expression and cell sensitivity to therapeutics

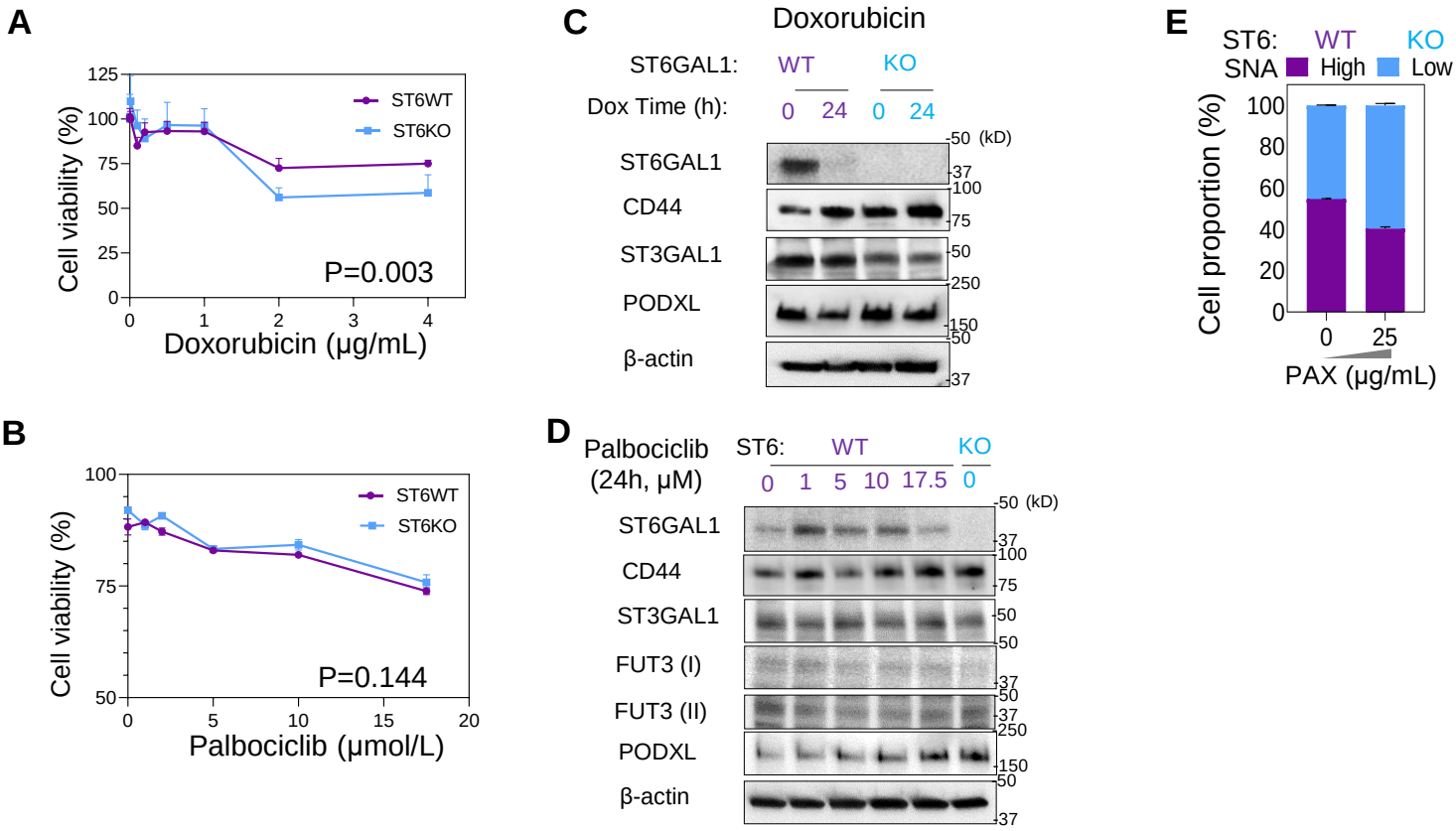

Supplementary Fig. S6. ST6GAL1 expression and cell sensitivity to therapeutic treatment (paclitaxel, doxorubicin, and palbociclib)

A-B. Cell viability (%) of MDA-MB-231 cells after treatments with 0-4 μg/mL doxorubicin (A) and 0-17.5 μmol/L palbociclib (B). P values are calculated with Student's *t*-test by Graphpad. Data are represented as mean of 6 (A) and 3 (B) experimental replicates.

C. Immunoblots using indicated antibodies with MDA-MB-231 ST6WT and ST6KO cell lysate prior to (0 h) and post (24 h) treatment with doxorubicin (Dox, 1μg/mL).

D. Immunoblots of MDA-MB-231 ST6WT and ST6KO cells after 24 h treatment of palbociclib at indicated doses.

E. Proportion (%) of α2,6-SA-high and -low cells within mixed ST6WT (SNA high) and ST6KO (SNA low) cells at 1:1, after 24 h treatment of PAX (0 and 25 μg/mL) ($p \leq 0.0001$). P values are calculated with Student's *t*-test in Graphpad. Data are represented as mean with ±SD of 3 experimental replicates.

Supplementary Figure S7. Altered pathways in ST6GAL1-KO cells

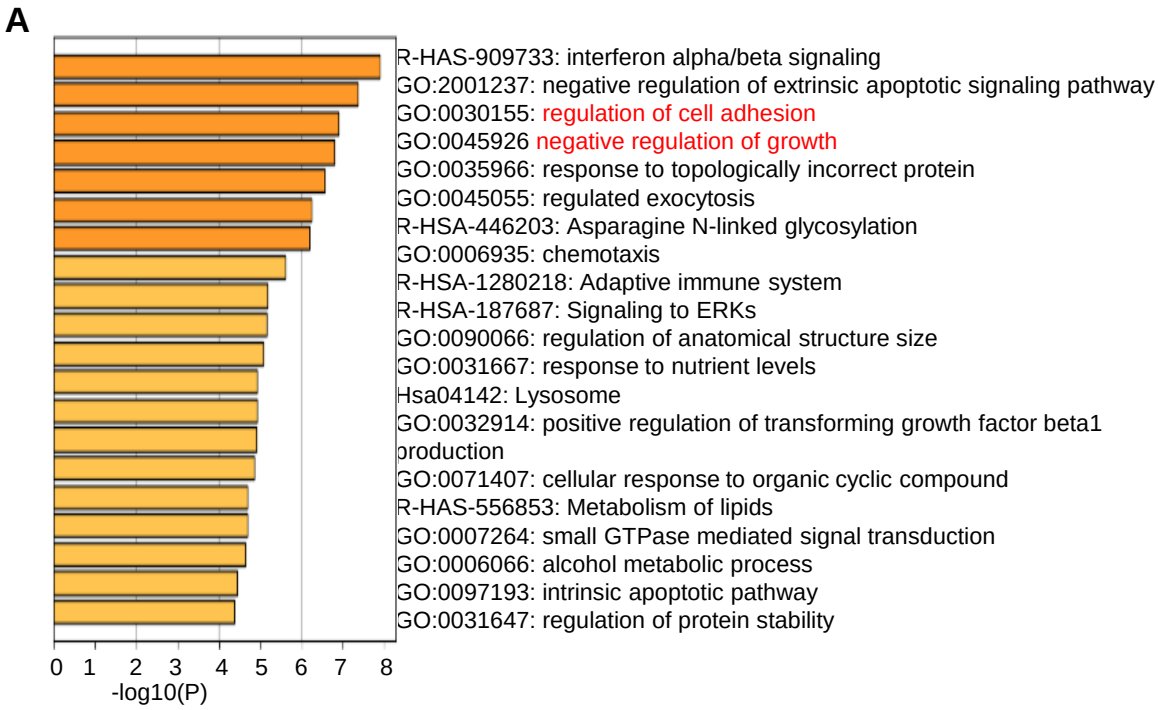

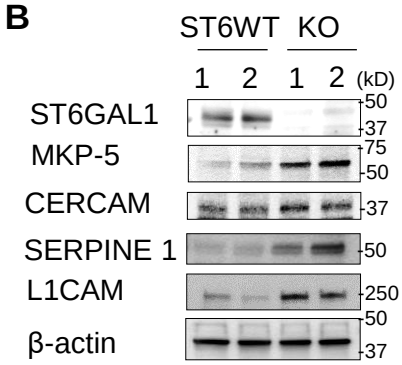

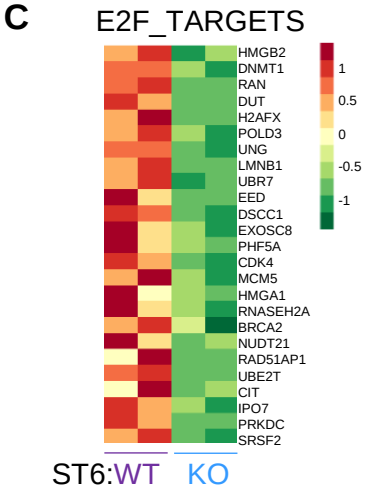

Supplementary Fig. S7. Altered pathways in ST6GAL1-KO cells (cell adhesion and E2F targets).

A. Pathway analysis of altered mRNAs in ST6KO MDA-MB-231 cells in comparison with ST6WT cells, detected by bulk tumor cell RNA sequencing, showing altered pathways of interferon alpha/beta signaling, cell adhesion, negative cell death, and negative growth.

B. Immunoblots of altered cell-adhesion molecules in ST6KO cells (MKP-5, CERCAM, SPERPINE1, and L1CAM).

C. Heat map of E2F target genes in ST6WT and ST6KO cells.

Supplementary Figure S8. ST6GAL1 is associated with cell growth and patient survival

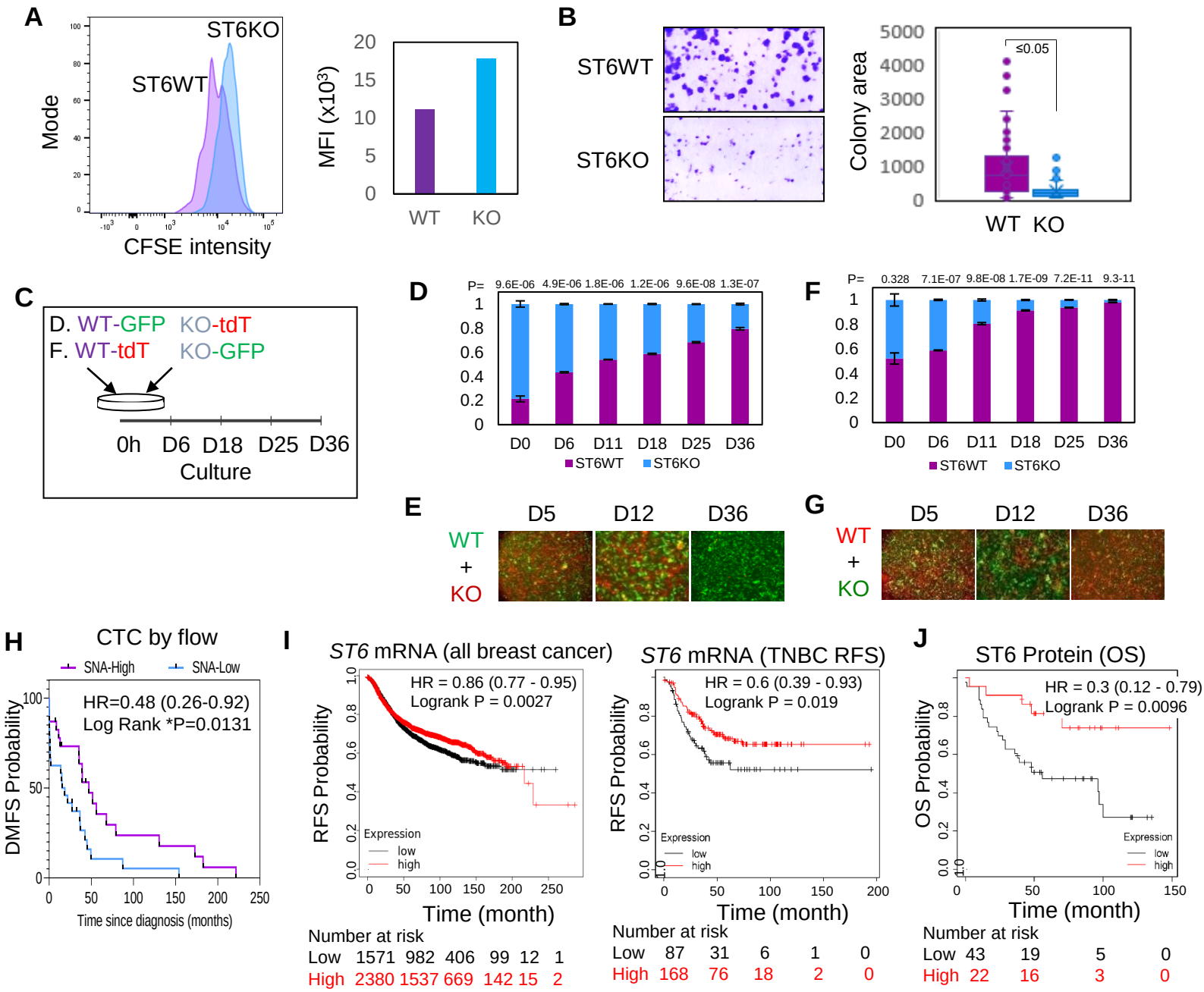

Supplementary Fig. S8. ST6GAL1 deficiency slows tumor cell growth and is associated with Kaplan Meier estimates of patient survival

A. Representative flow cytometry profile (left panel) and bar graph (right panel) of MFI for carboxyfluorescein succinimidyl ester (CFSE) staining of ST6WT and ST6KO MDA-MB-231 cells for cell division analysis.

B. Representative images (left panels) and bar graph of the colony size (right panel) of ST6WT and ST6KO cells;. Colony size were measured using ImageJ. P values are calculated using Student's *t*-test via Excel. Data are represented as mean values +/- SD.

C. Experimental illustration of cell growth-competition with 20% L2G-WT and 80% L2T-KO cells (D-E) or 50% L2T-ST6WT (WT) and 50% L2G-ST6KO (KO) or were mixed and plated. Cells (%) with respective colors were counted on indicated days using flow cytometry.

D-G. Quantification (D and F) and representative fluorescence images (E and G) of mixed ST6WT and ST6KO cells on indicated days. Student's *t*-test P values are indicated for each mixed pair over the measured days.

H. The probability of distant metastasis-free survival (DMFS) in breast cancer (N=50, median cutoff for the patient groups of SNA high and low, with >10 CTCs or ≤10 CTCs of SNA high expression, Log rank P=0.013).

I-J. The probability of relapse-free survival (RFS) (I) or overall survival (OS) (J) by Kaplan-Meier plotter in all breast cancer (N = 3951, log rank P = 0.0027, q = 0.0182) and in TNBC (N=255, log rank P = 0.019) by mRNA expression (I) and by protein expression in breast cancer bearing patients (N = 65, P = 0.0096) (J).

Supplementary Figure S9. Dynamic glycosylation profile in CTCs of PDXs and tumor models.

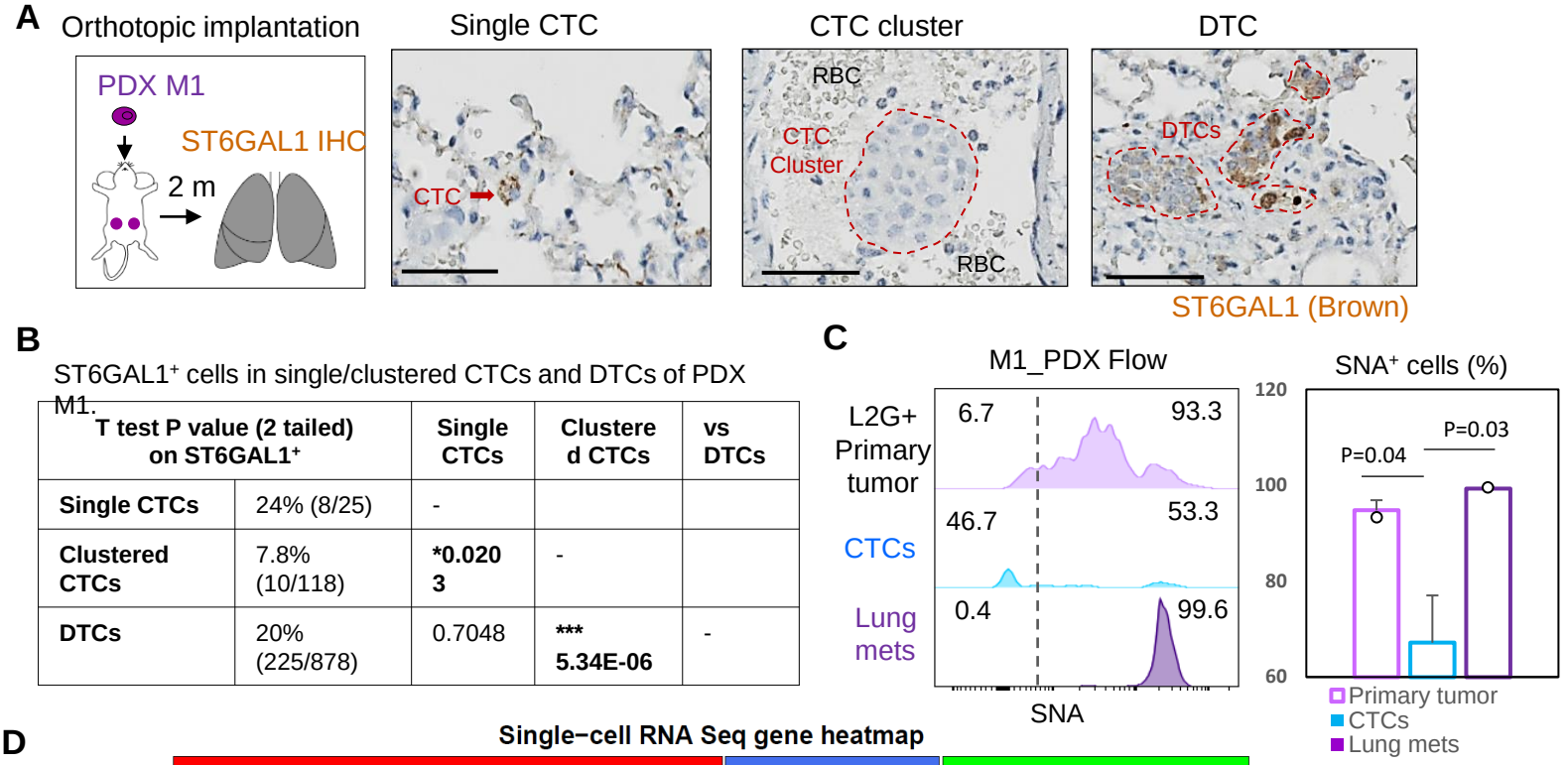

Supplementary Fig. S9. Dynamic glycosylation profile in CTCs of PDXs and tumor models.

A-B. Schematic of orthotopic PDX-M1 tumors and representative lung images (A) and table (B) of ST6GAL1 positivity (brown) in single CTC ($ST6GAL1^{+}$), CTC cluster ($ST6GAL1^{-}$) within the vasculature in situ (surrounded by non-clear red blood cells [RBCs]) and disseminated tumor cells (DTCs) (mixed $ST6GAL1^{+/-}$) in the parenchyma. Scale bar = 50 μm, nuclear DNA stained in blue. $ST6GAL1^{+}$ cells (%) within single CTCs, CTC clusters, and DTCs and the Student's *t*-test P values of each comparison between CTCs (singles and clusters) and DTCs, calculated via GraphPad.

C. Flow cytometry profiles (left two panels) and quantified bar graph (right panel) of SNA signals (α2,6-SA levels) in PDX-M1 primary tumor cells, decreased in CTCs, and restored in lung metastases. Biological replicates are included in the bar graph, two tailed Student's *t*-test for two comparisons P=0.04 and 0.03 respectively.

D. Heat map of single-cell RNA seq transcriptome of eGFP+ or tdTomato+ primary tumor cells, CTCs, and lung metastatic cells sorted from TNBC PDX- and MDA-MB-231 tumor-bearing mice. ST6GAL1 was detected in a few cells of primary tumor cells and lung mets but was not detected in CTCs.

E. The schematic of tail vein injection of sorted α2,6-SA-high and -low MDA-MB-231 cells (L2G or L2T-labeled). Mice were sacrificed for lung dissection on Day 1 (D1, 24 h) and Day 9 (D9, 9 days) after intravenous injections.

F. Flow profiles of sorted SNA-high and low cells on Day 0 (D 0) prior to tail vein injection, representative images of lung BLI (1 h), lung *ex-vivo* BLI (24 h and D 9), and flow profiles of α2,6-SA levels in the tumor cells disseminated to the lungs, and a bar graph of SNA high cells disseminated to the lungs on D9 as measured via flow cytometry.

Supplementary Figure S10. ST6GAL1 suppresses the seeding (related to Fig 4).

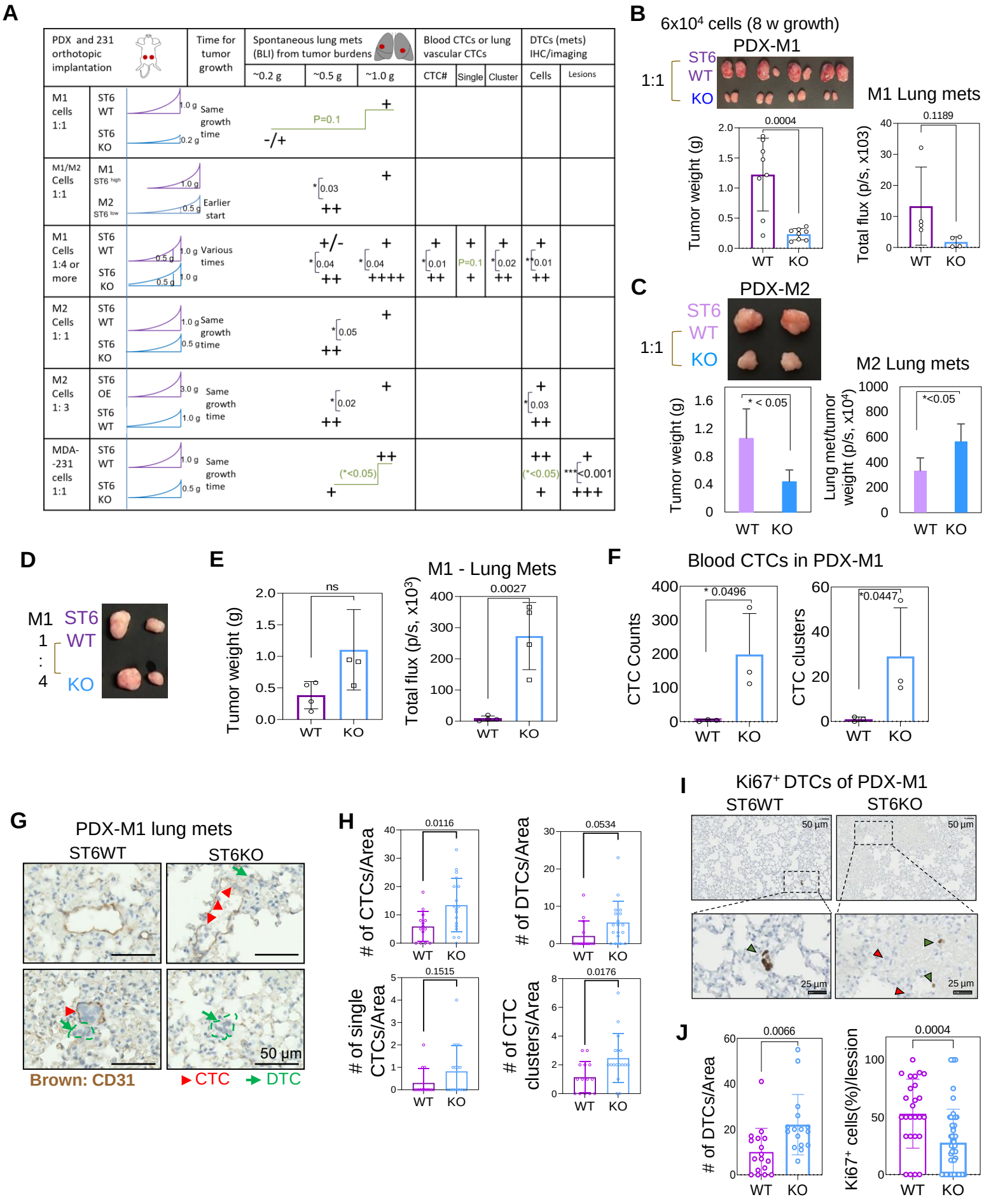

Supplementary Fig. S10. ST6GAL1 suppresses the seeding of lung metastasis in PDX and tumor models. (related to Fig 4).

A. Summary table of PDX (M1 and M2) and MDA-MB-231 orthotopic tumor models, implanted in comparison pairs of ST6WT and ST6KO cells, ST6 high (M1) and ST6 low (M2), or ST6 WT and ST6OE (M2) cells at the same ratio (1:1) or different ratios (1:3, 1:4 or more) for various periods of times for tumor growth and analyses of spontaneous metastases to the lungs via bioluminescence imaging (BLI), immunohistochemistry straining of CTCs and disseminated tumor cells (DTCs) within and outside the $CD31^+$ vasculature, respectively, in the lung sections of tumor-bearing mice.

B. PDX-M1 tumor images (top left panel), quantified weight of tumors (bottom left panel), and spontaneous lung metastases measured via BLI *ex vivo* (right panel), developed within 8 weeks after orthotopic implantations of 6e+4 tumors cells, at 1:1 ratio for ST6WT and ST6KO (N=4 mice of 8 tumors for each group).

C. PDX-M2 tumor images (ST6WT and KO) (top left panel), tumor weight (bottom left panel), and lung metastases via BLI *ex vivo* (right panel), at two months after orthotopic implantation with the same numbers of cells, or at the ratio of 1:1, into 4th mammary fat pads. The quantification of lung metastasis of ST6WT and ST6KO of PDX-M2 was normalized with tumor weight. Student's *t*-test *$p < 0.05$. Data are represented as mean values +/- SD.

D-F. $L2G^+$ or $L2T^+$ PDX-M1 tumor images (D top panel), quantified weight of tumors (D bottom panel), and spontaneous lung metastases measured via BLI *ex vivo* (E, normalized with tumor weight), developed within 8 weeks after orthotopic implantations of ST6WT tumor cells (1.2e+4) and ST6KO cells (5e+4) cells, at 1:4 ratio (N=4 mice of 8 tumors for each group). Total $eGFP^+$ or $tdTomato^+$ CTC counts (left panel) and CTC clusters (right panel) in the blood of each mouse were measured via flow cytometry (F).

G. Representative lung images with CD31 IHC (brown) of ST6WT and ST6KO PDX-M1 tumor bearing mice. Scale bar=50 μm, CTCs (clusters) indicated with red arrow heads, and DTCs are pointed with green arrows.

H. Quantification of CTCs (within the $CD31^+$ vasculature) and DTCs (outside the vasculature) in the lungs of ST6WT and ST6KO PDX-M1-bearing mice. The number of CTCs (single and clustered) per lung image area and number of DTCs per image area are presented in ST6WT and ST6KO groups. Indicated Student's *t*-test P values are calculated by GraphPad. The data are represented with +/-SD of 15 (WT) and 18 (KO) images.

I-J. The representative Ki67 IHC images (I) and bar graphs of lung metastases (# of DTCs/lesion, and % of $Ki67^+$ cells/lesion) (J) from PDX-M1 ST6WT and ST6KO tumor bearing mice. Nuclei in blue and Ki67 in brown, scale bar=25 or 50 μm as indicated. P values are calculated with Student's *t*-test using GraphPad. Data are represented as mean +/- SD of 3-4 biological replicates and 17 experimental replicates.

Supplementary Figure S11. Counts and Ki67 expression of CTCs and DTCs in situ.

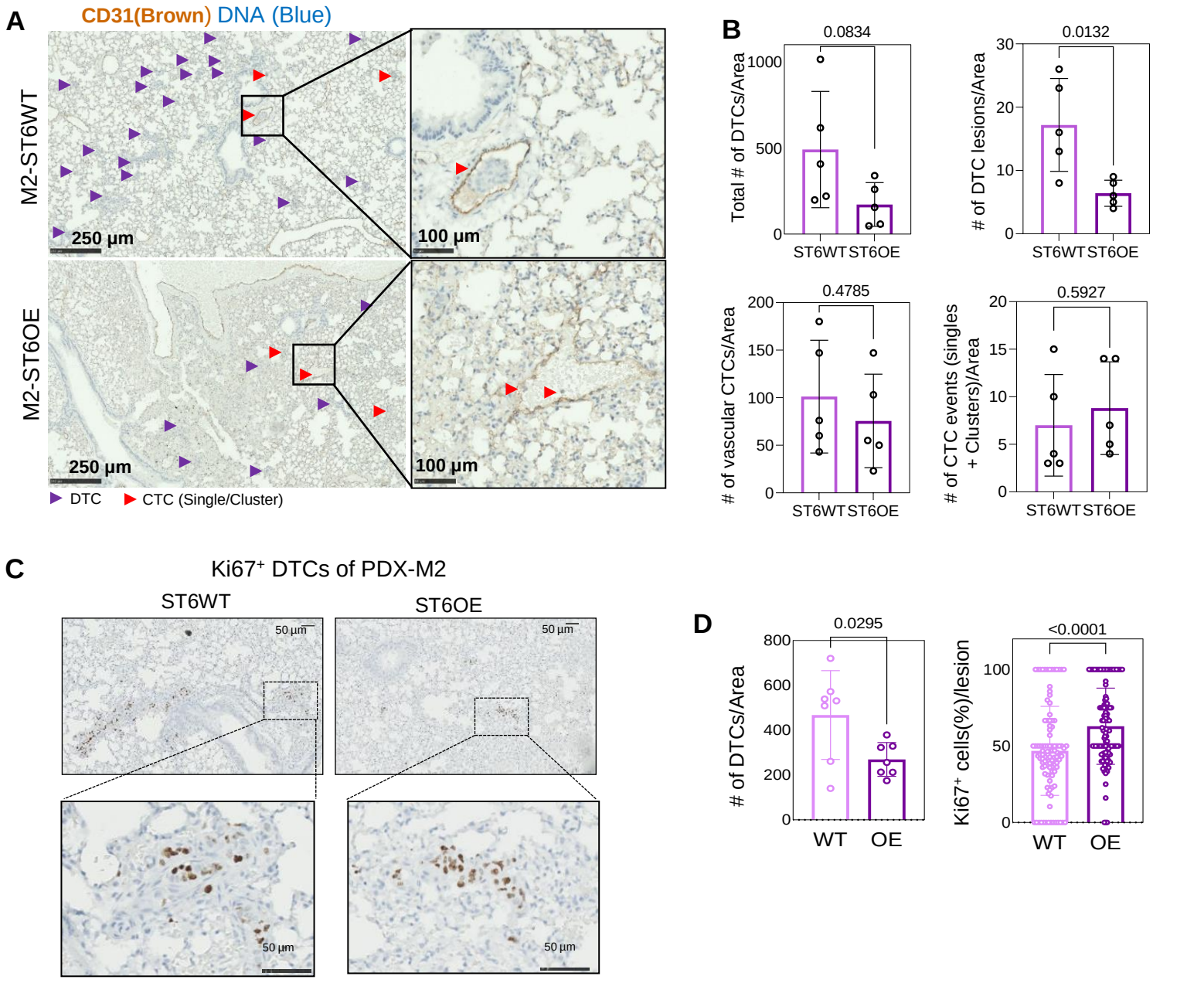

Supplementary Fig. S11. Counts and Ki67 expression analyses of CTCs and DTCs in situ in the mouse lung sections of the mice bearing ST6WT and ST6OE PDXs.

A-B. Representative lung images with CD31 IHC staining and pointed CTCs (red heads)/DTCs (purple heads) (B), and bar graphs (C) of vascular CTCs, and extravascular DTCs in PDX-M2 models of ST6WT and ST6OE after orthotopic implantation at a cellular ratio of 3:1, as shown in **Fig 4M**.

C-D. The representative Ki67 IHC images (C) and bar graphs of lung metastases (# of DTCs/lesion, and % of Ki67⁺ cells/lesion) (D) from PDX-M1 ST6WT and ST6OE tumor bearing mice. Nuclei in blue and Ki67 in brown, scale bar=25 or 50 μm as indicated. P values are calculated with Student's *t*-test using GraphPad. Data are represented as mean +/- SD of 3-4 biological replicates and 17 experimental replicates.

Supplementary Figure S12. ST6GAL1 KO promotes transendothelial migration / seeding

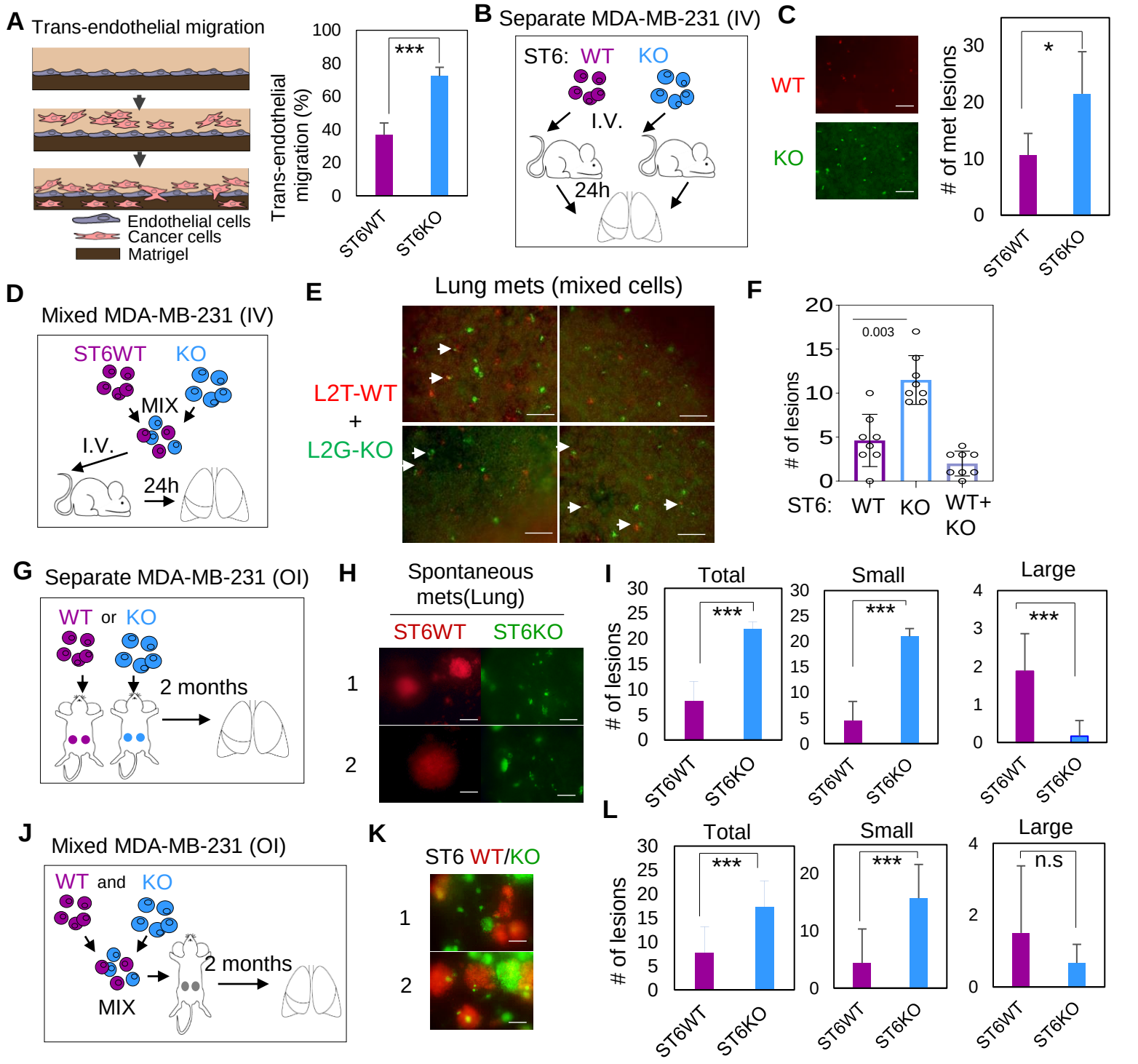

Supplementary Fig. S12. Depletion of ST6GAL1 promotes transendothelial migration and seeding.

A. Schematic of the tumor cell trans-endothelial migration (TEM) assay (left panel) and quantification of ST6WT and ST6KO MDA-MB-231 tumor cells migrated through HUVEC (%).

B-F. Illustrations of tail vein injection of ST6WT (L2T)) and ST6KO (L2G) MDA-MB-231 cells separately (B) or in mixture of both cells (D). $5x10^4$ cells were injected. Seeding to the lungs were measured under fluorescence microscope at 24 h after injections. Representative images of metastatic seeds of ST6WT (red) and ST6KO (green) and the quantifications are shown in C, E, and F. In mixture injected mice, homotypic colonies (WT or KO) and heterotypic colonies (WT+KO) of metastasis are quantified (F). Student's *t*-test P values are calculated via GraphPad (C, F).

G-L. Illustrations of orthotopic injections of ST6WT (red, L2T)) and ST6KO (green, L2G) MDA-MB-231 cells separately (G) or in mixture of both cells (J). For both single and mixed populations, $1x10^4$ cells were injected. Representative images of metastasis of ST6WT (red) and ST6KO (green) (H, K) and the quantifications (I, L) in which total, small, and large lesions of metastases in the lungs are counted.

Student's *t*-test, n.s = not significant, ***p < 0.001, *p≤0.05 by Excel calculation. Data are represented as mean values of 3-5 biological replicates with +/- SD. Scale bars=200μm

Supplementary Figure S13. CD44 is α2,6-sialylated by ST6GAL1

A CD44 amino acid sequences the green peptides pulled down by SNA and detected by mass spec

CD44 peptides by SNA-IP and mass spec

>sp|P16070|CD44_HUMAN CD44 antigen OS=Homo sapiens OX=9606 GN=CD44 PE=1 SV=3

```
        10        20        30        40        50        60        70        80        90       100
MDKFWWHAAWGLCLVPLSLAQIDLNITCRFAGVFHVEKNGRYSISRTEAADLCKAFNSTLPTMAQMEKALSIGFETCRYGFIEGHVVIPRIHPNSICAAN
       110       120       130       140       150       160       170       180       190       200
NTGVYILTSNTSQYDTYCFNASAPPEEDCTSVTDLPNAFDGPITITIVNRDGTRYVQKGEYRTNPEDIYPSNPTDDDVSSGSSSERSSTSGGYIFYTFST
       210       220       230       240       250       260       270       280       290       300
VHPIPDEDSPWITDSTDRIPATTLMSTSATATETATKRQETWDWFSWLFLPSESKNHLHTTTQMAGTSSNTISAGWEPNEENEDERDRHLSFSGSGIDDD
       310       320       330       340       350       360       370       380       390       400
EDFISSTISTTPRAFDHTKQNQDWTQWNPSHSNPEVLLQTTTRMTDVDRNGTTAYEGNWNPEAHPPLIHHEHHEEEETPHSTSTIQATPSSTTEETATQK
       410       420       430       440       450       460       470       480       490       500
EQWFGNRWHEGYRQTPKEDSHSTTGTAAASAHTSHPMQGRTTPSPEDSSWTDFFNPISHPMGRGHQAGRRMDMDSSHSITLQPTANPNTGLVEDLDRTGP
       510       520       530       540       550       560       570       580       590       600
LSMTTQQSNSQSFSTSHEGLEEDKDHPTTSTLTSSNRNDVTGGRRDPNHSEGSTTLLEGYTSHYPHTKESRTFIPVTSAKTGSFGVTAVTVGDSNSNVNR
       610       620       630       640       650       660       670       680       690       700
SLSGDQDTFHPSGGSHTTHGSESDGHSHGSQEGGANTTSGPIRTPQIPEWLIILASLLALALILAVCIAVNSRRRCGQKKLVINSGNGAVEDRKPSGLN
       710       720       730       740
GEASKSQEMVHLVNKESSETPDQFMTADETRNLQNVDMKIGV
```

B

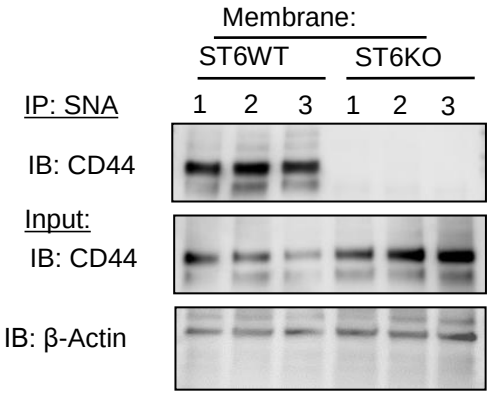

Supplementary Fig. S13. CD44 is α2,6-sialylated by ST6GAL1.

A. Amino acid sequence coverage of CD44 from SNA pull down of ST6WT lysates, detected by LC-MS/MS.

B. The validation of CD44 sialylation by co-immunoprecipitation assay. Mambrane fractions were isolated from three different clones of ST6WT and ST6KO MDA-MB-231 cells. SNA bound agarose beads were used to pull down SNA-binding peptides.

Supplementary Figure S14. ST6GAL1 targets in clusters with altered binding affinity

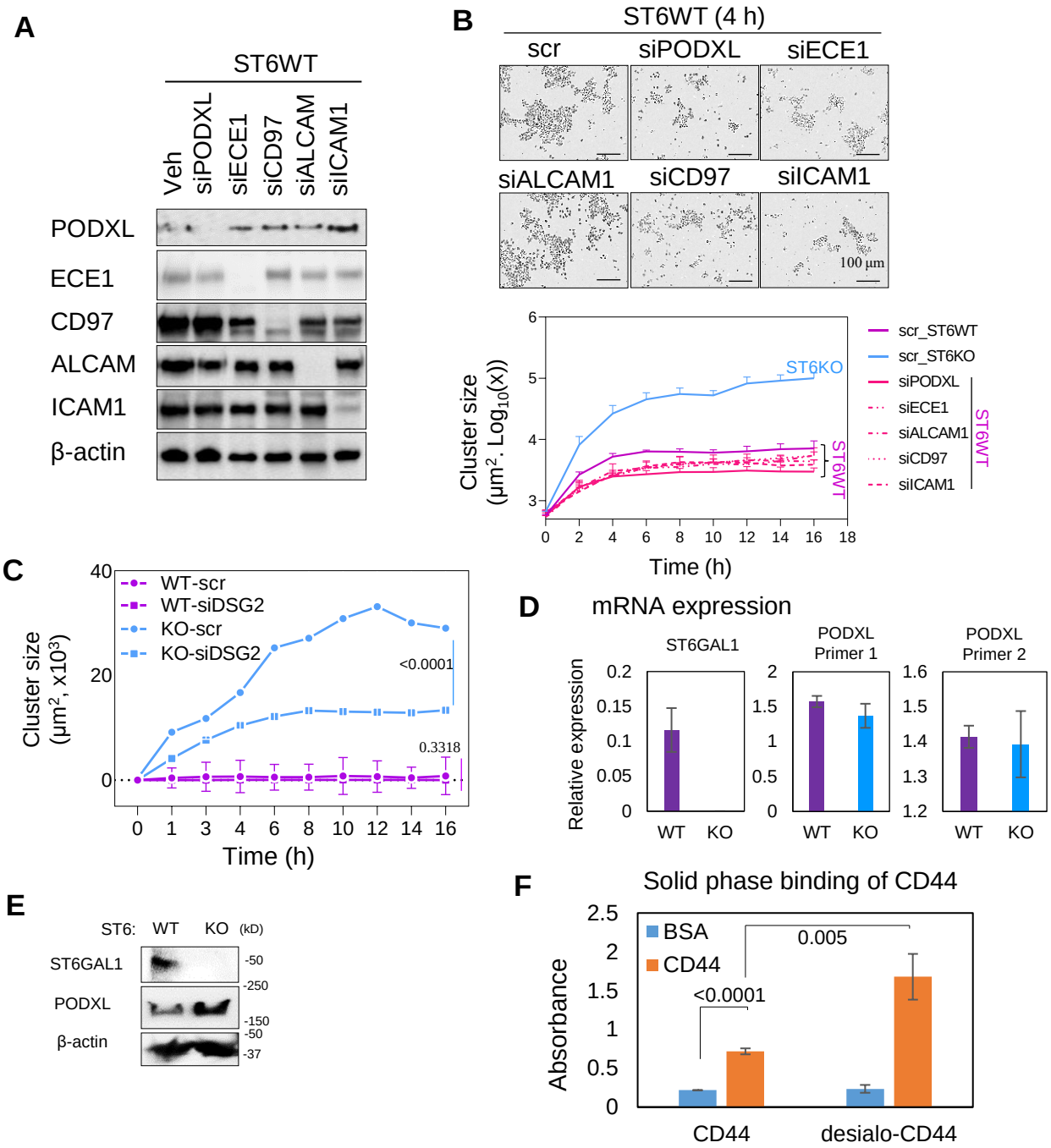

Suppl. Fig. S14. Down-regulation of ST6GAL1 target genes reduces cluster formation and de-sialylation of targets increases binding affinity.

A. Immunoblots of down-regulated ST6GAL1 target proteins (PODXL, ECE1, CD97, ALCAM, and ICAM1) and the loading control β-actin from the lysates of ST6WT MDA-MB-231 cells transfected with siRNAs for PODXL, ECE1, CD97, ALCAM1, and ICAM1.

B. Representative images (top left panels, scale bar = 100 µm), cluster formation curves over time (bottom left panel), and cell counts (top right panel) of ST6WT MDA-MB-231 cells after knockdown of indicated genes by respective siRNAs. scr; scrambled control RNA. scr; scrambled control siRNA ($P_{scrST6WT\ vs\ KO}$<0.0001, $P_{scrST6WT\ vs\ siPODXL}$<0.0001, $P_{scrST6WT\ vs\ siECE1}$=0.0060, $P_{scrST6WT\ vs\ siALCAM1}$=0.3232, $P_{scrST6WT\ vs\ siCD97}$=0.0347, $P_{scrST6WT\ vs\ siICAM1}$ =0.0135. P values are calculated with Student's *t*-test by GraphPad. Data are represented as mean +/- SD of 12 experimental replicates. Cluster videos are attached as Suppl. Video 15-20.

C. The cluster curve of ST6WT (WT, purple) and ST6KO (KO, blue) cells with srambled siRNA control (scr) and siDSG2 knockdown.

D-E. The mRNA expression levels of ST6GAL1 and PODXL, measured by RT-PCR with different primers (E), and immunoblots of protein expression of ST6GAL1 and PODXL (F) in ST6WT and ST6KO cells.

F. Improved solid phase binding of recombinant CD44 in homophilic CD44-CD44 interactions after neuraminidase treatment. BSA was used as a negative control.

Supplementary Figure S15. ST6GAL1 substrates regulate metastatic seeding

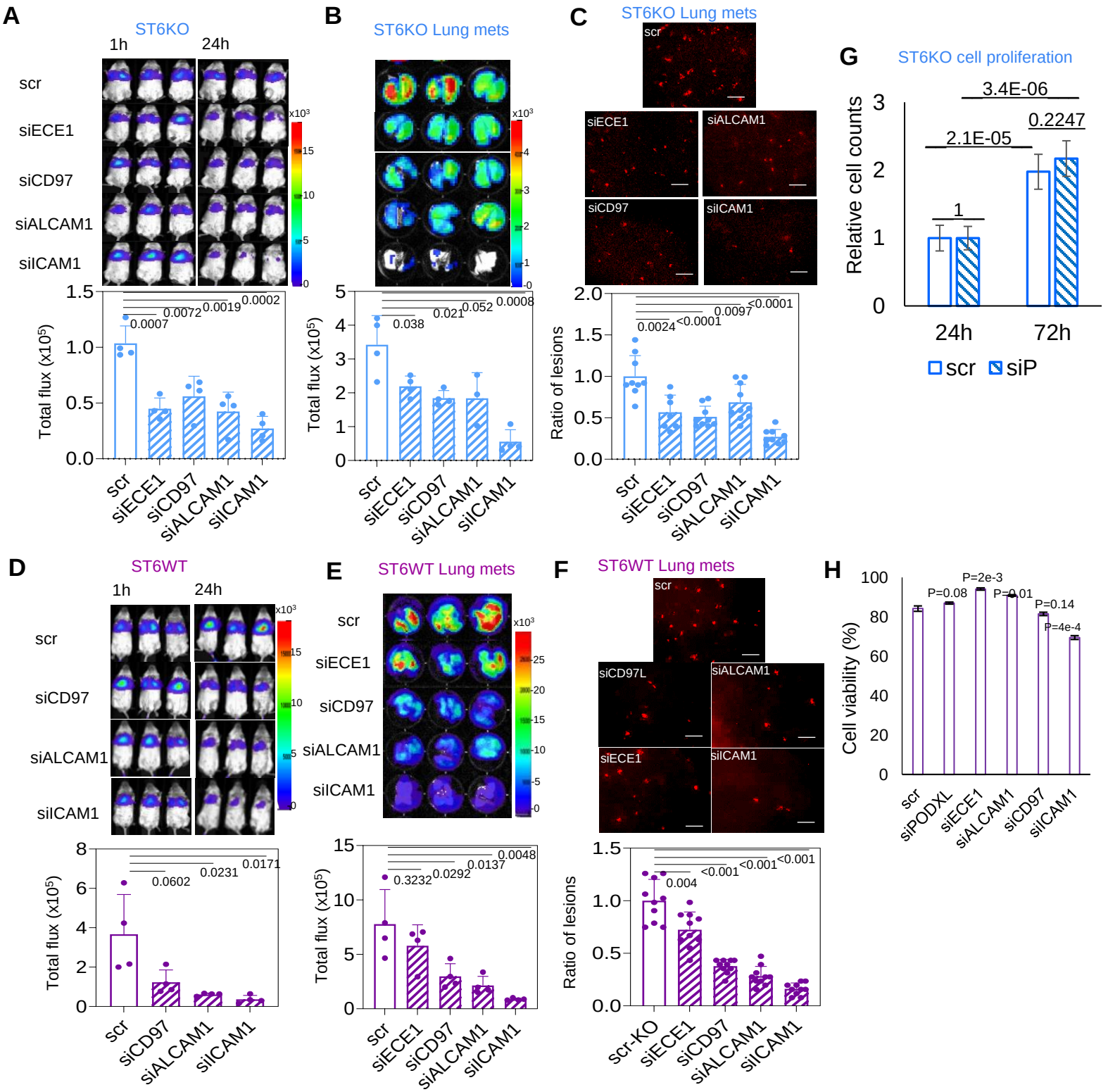

Supplementary Fig. S15. Down-regulation of ST6GAL1 substrates inhibits metastatic seeding.

A-F. Metastatic seeding of ST6KO cells (A-C) and ST6WT cells (D-F) after knockdown of the indicated genes after siRNA transfections. Mouse bioluminescence images (BLI) (A and D), lung ex-vivo BLI (B and E) and metastatic lesions under fluorescence microscope (C and F) are shown with the representative images (top panels) and quantifications (bottom panels). Scale bar = 100µm, P values are calculated using Student's *t*-test via GraphPad. Data are represented as mean +/- SD of 4 biological replicates.

G-H. Cell counts of ST6KO cells (G) and the cell viability (%) (H) of MDA-MB-231 cells after two transfections with scrambled control (scr) andeach of the indicated siRNAs, siPODXL (siP), siECE1, siCD97, and siICAM1, measured by hematometer counting and DAPI exclusion (flow cytometry), respectively.

Supplementary Figure S16. anti-PODXL antibody inhibits cluster formation and seeding

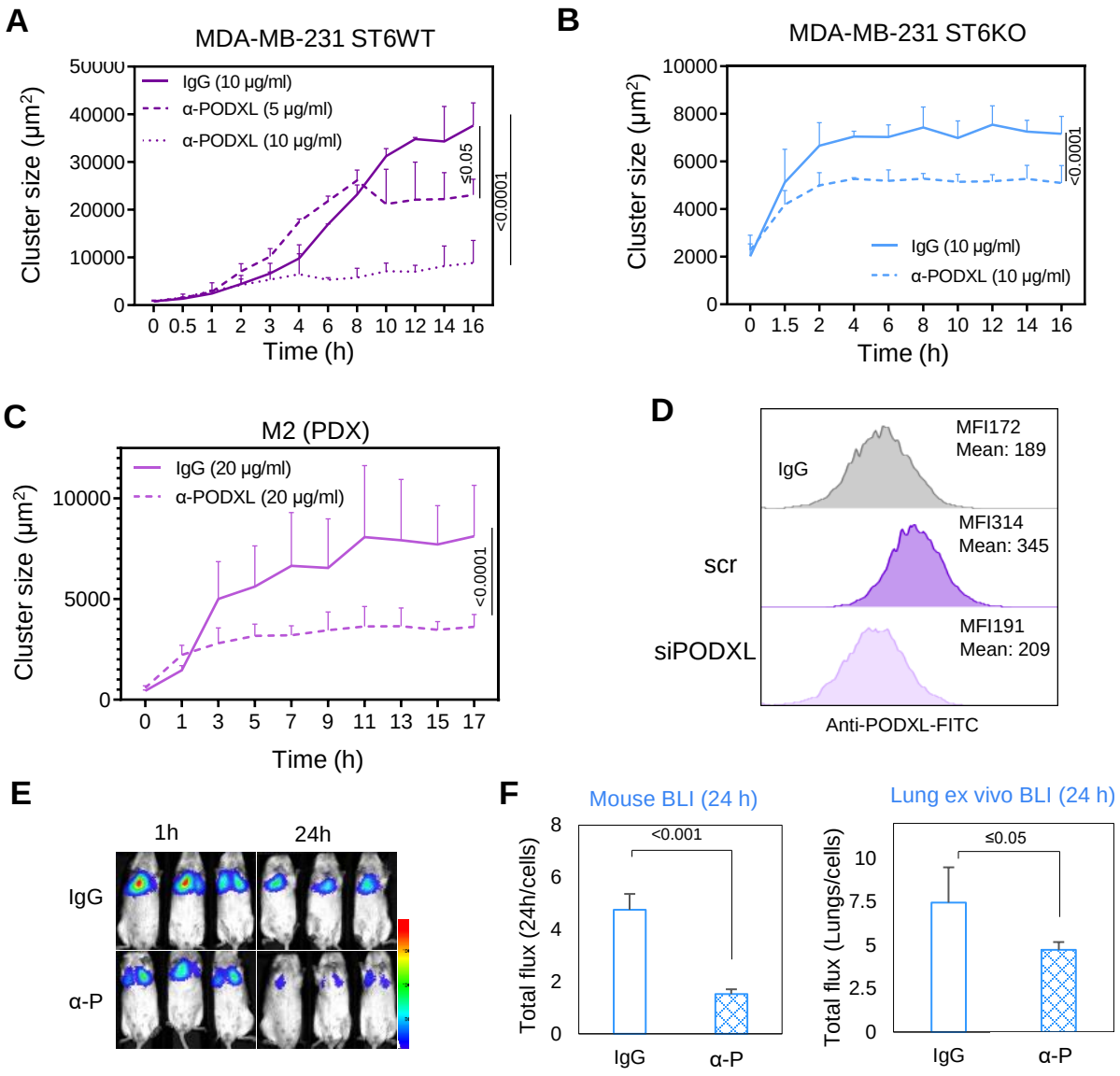

Supplementary Fig. S16. anti-PODXL antibody treatment inhibits tumor cluster formation and metastatic seeding (related to Fig 5).

A. Cluster formation curve of ST6WT MDA-MB-231 cells ($2x10^4$ cells/well) after anti-PODXL and IgG treatment at indicated doses.

B. Cluster formation curves of ST6KO MDA-MB-231 cells ($1.5x10^4$ cells/well) after anti-PODXL treatment in comparison with the IgG isotope control.

C. Cluster formation assay of PDX-M2 tumor cells after anti-PODXL and IgG treatment.

D. Representative flow profiles of the conjugated anti-PODXL-FITC binding to MDA-MB-231 cells after transfections with srambled siRNA control (scr) and siPODXL knockdown.

E-F. Representative images of mouse BLI (E) and the quantifications of BLI in mice (F, left panel) and the lungs ex vivo (F, right panel) after administration of anti-PODXL neutralizing antibody to ST6KO MDA-MB-231 cells. Cells were pre-incubated with anti-PODXL antibody or isotope control IgG. BLI was performed at 1 h and 24 h after tail vein injection. The normalized fold change was calculated as the total flux of images divided by the total flux of injected cells.

Significance are calculated with Student's *t*-test using GraphPad. Data are represented as mean +/- SD of 3-4 experimental replicates.

Supplementary Figure S17. Anti-PODXL effects on CTCs and seeding of PDX-M1

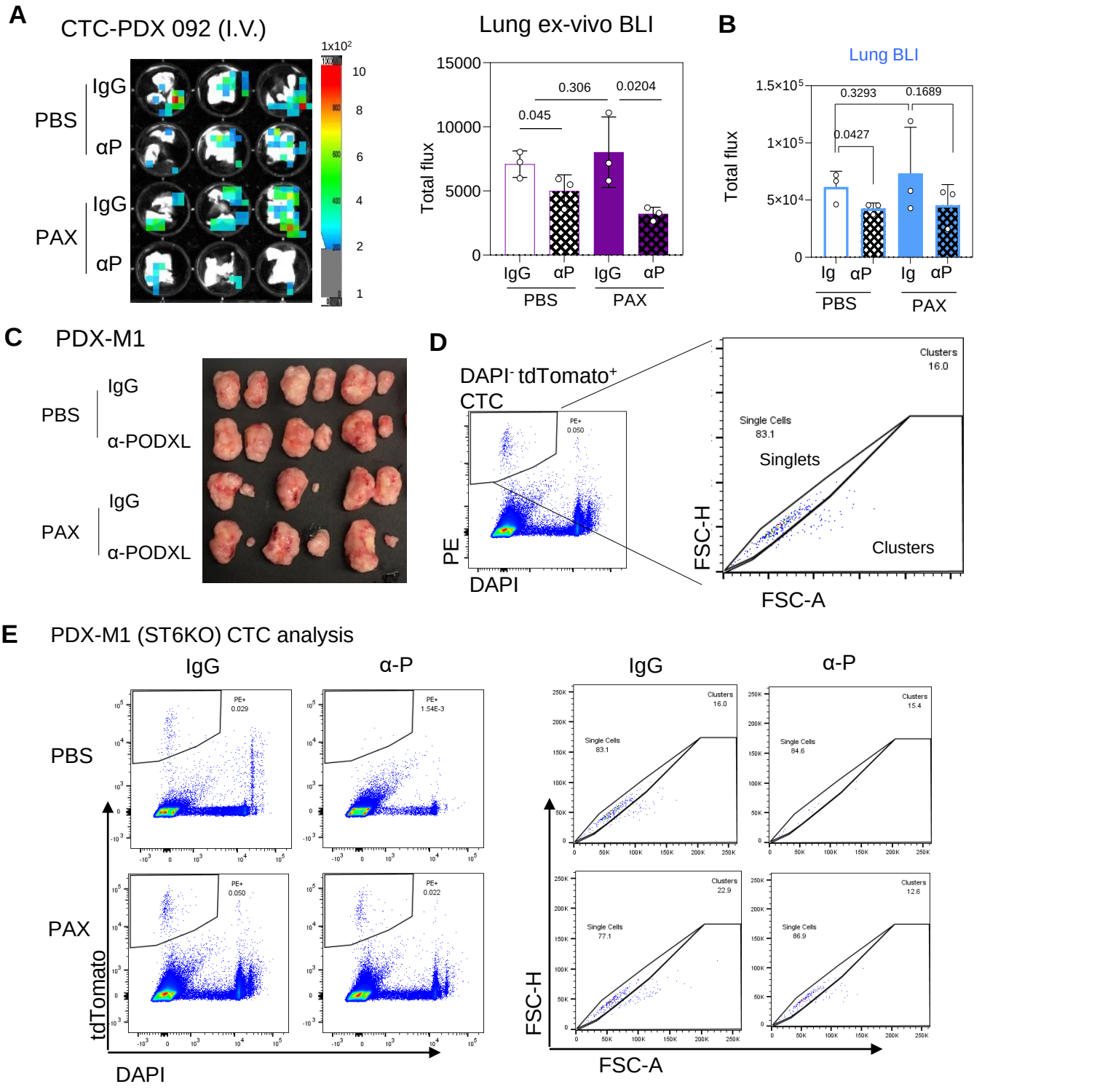

Supplementary Fig. S17. Anti-PODXL effects on the metastatic seeding of PDX-M1 tumors after PAX-treatment and the gating strategy of flow analysis of CTCs (related to Fig 5).

A. Representative images of lung ex-vivo BLI and bar graph quantification of CTC-PDX 092 tumor cells inoculated via tail vein to NSG mice. Cells were pre-treated with indicated combinations of drugs (PAX (NAB) (50 μg/ml) or PBS with αP or IgG control (20 μg/mL) for 12 hour prior to inoculation. mice were treated with the same combination of drugs (PAX-NAB, 27 mg/kg or PBS, αP or IgG control, 30 μg/mouse) via tail vein 3 h prior to cell inoculation via tail vein (IV). Lung ex-vivo BLIs were measured after 3 weeks. Student's *t*-test P values are calculated by GraphPad. Data are representative of 3 biological replicates and shown with +/- SD.

B. Non-normalized raw bioluminescence signals of PDX-M1 lung metastases after PAX and α-P treatment in Fig 6M.

C. Images of breast tumors in indicated treatment groups.

D. Gating strategy of tdTomato⁺Dapi (viable) CTCs in the blood of PDX-M1 tumor (tdTomato labeled) bearing mice.

E. Representative images of tdTomato⁺ CTCs (left panels) and separation of single versus clustered CTCs (right panels) in each group.